Environmental Science Processes & Impacts

ROYAL SOCIETY OF CHEMISTRY

PAPER

View Article Online
View Journal

Cite this: DOI: 10.1039/d5em01004g

Visible radiation-driven photomineralization and photoproduction of dissolved organic matter in a large estuary: implications for coastal ocean biogeochemical cycles

Guisheng Song, *[a] Fuxin Niu,[b] Yao Gong,[b] Philippe Massicotte,[c] Han Zuo,[a] Mengting Li[a] and Huixiang Xie *[d]

Photochemistry can convert dissolved organic matter (DOM) to inorganics (mainly CO_2) and "new" DOM, hence impacting aquatic carbon cycling. The apparent quantum yields (AQYs) of these photoprocesses usually decrease with increasing wavelength. This study reports exceptions to this paradigm and discusses the biogeochemical implications of this phenomenon. Specifically, we determined the broadband AQYs over ultraviolet-B (UVB), ultraviolet-A (UVA), and visible (VIS) radiations for photomineralization of dissolved organic carbon (DOC) and photobleaching of chromophoric and florescent DOM (CDOM, FDOM) in the freshwater, brackish water, and seawater samples from the Pearl River estuary. UVB-broadband AQYs of DOC photomineralization (AQY_{DOC}) and of CDOM and humic-like FDOM photoleaching were considerably higher than their UVA and VIS counterparts for all three water samples. Surprisingly, the broadband AQY_{DOC} over VIS was significantly higher than that over UVA for the brackish water and seawater samples, contrary to the above-mentioned paradigm. Moreover, exposure of all three water samples to VIS produced protein-like FDOM, while significant losses of this FDOM pool occurred in the presence of UV. Per depth-integrated contributions in the water column, UVB or UVA primarily controlled CDOM and FDOM photobleaching, while VIS dominated DOC photomineralization and protein-like FDOM formation. These results suggest photochemistry may cause CO_2 and biolabile DOM accumulations in VIS-dominated sunlit waters below surface mixed layers, contributing to coastal ocean DOM biogeochemical cycling, acidification, and deoxygenation. This shall be a self-intensified process since UV-driven CDOM photobleaching in surface layers reinforces and extends further deeper the VIS-induced subsurface CO_2 and biolabile DOM photoproduction.

Received 3rd December 2025
Accepted 29th March 2026

DOI: 10.1039/d5em01004g

rsc.li/espi

Environmental significance

Sunlight-driven photoreactions can photobleach and photomineralize dissolved organic matter (DOM), and produce more biolabile DOM. The efficiencies of DOM photoreactions usually decrease with increasing light wavelength. This study, however, demonstrates that visible light (VIS) dominates DOM photomineralization and photoproduction of proteinaceous (biolabile) DOM, while ultraviolet radiation (UV) mainly controls DOM photobleaching. As both photomineralization and microbial degradation of DOM consume oxygen and form CO_2, VIS-induced photoreactions may cause CO_2 and biolabile DOM accumulations in subsurface waters where VIS can reach but UV is absent, thereby contributing to subsurface DOM cycling, acidification, and oxygen depletion in coastal oceans. This shall be a self-intensified process since UV-induced DOM photobleaching in surface waters allows more VIS to reach subsurface waters.

1 Introduction

Dissolved organic matter (DOM) plays a crucial role in global carbon cycling and climate change.[1] The chromophoric fraction of DOM (CDOM) absorbs solar ultraviolet (UV) and visible (VIS) radiation, while the fluorescent constituent of DOM (FDOM) emits fluorescence upon absorbing light.[2] Based on its fluorescence excitation–emission characteristics, FDOM can be further classified into humic-like and protein-like components,[3] with the former being largely bio-refractory and the latter biolabile. In sunlit waters, CDOM undergoes photochemical transformations with biogeochemical and optical ramifications, including photomineralization (*i.e.*, conversion of dissolved organic carbon (DOC) into CO_2 and CO), photobleaching of chromophores and fluorophores, which increases water transparency, and photoproduction of biolabile

[a]Tianjin Key Laboratory for Marine Environmental Research and Service, School of Marine Science and Technology, Tianjin University, Tianjin, China. E-mail: guisheng.song@tju.edu.cn
[b]Tianjin Ocean Center, Ministry of Natural Resources, Tianjin, China
[c]CNRS, Université Laval, Sorbonne Université, Laboratoire de recherche international Takuvik, Québec, Canada
[d]Institut des sciences de la mer, Université du Québec à Rimouski, Rimouski, Québec, Canada. E-mail: huixiang_xie@uqar.ca

DOM,[4] including protein-like FDOM.[5–9] CDOM photomineralization alone or coupled with microbial uptake of photoproduced biolabile DOM is considered as an important DOM sink in marine ecosystems.[10–14] Moreover, as both DOC photomineralization and microbial oxidation of photoproduced biolabile DOM produce CO_2 and consume O_2, DOM photochemistry may affect natural waters' pH and oxygen content.[15–17]

DOM photoreactivity to a large extent is controlled by its source of formation, with terrestrial DOM generally being more susceptible to photomineralization and photobleaching than DOM of mainly marine origin.[18–21] Different DOM fractions may, however, display varying photochemical susceptibilities. For instance, humic-like FDOM fluorescence photobleaching was observed to be faster than CDOM absorbance photobleaching, followed by DOC photomineralization, for DOM collected from marine waters,[9,22] river plume waters,[7] lake waters,[23] and cyanobacteria cultures.[24] Furthermore, certain trace metals (*e.g.*, iron) may enhance the DOM photoreactivity.[25–28]

DOM photoreactivity is also sensitive to the wavelength of solar radiation initiating the photoprocesses. The efficiencies (*i.e.*, apparent quantum yields, AQYs) of DOM photoprocesses, including DOC photomimeralization and CDOM photobleachng, usually decrease with increasing wavelength,[18,29–35] which, combined with increasing solar irradiance with wavelength, leads to UVA often playing a central role in DOM photoreactions among the three solar spectral regimes (UVB: 290–320 nm; UVA: 320–400 nm; and VIS: 400–700 nm).[31,34,36–39] Here, we report exceptions to this traditional view of the wavelength dependence of DOM photoreactions based on water samples collected from the Pearl River Estuary (PRE).

The Pearl River, located in southeastern China, is the 13th largest world river based on freshwater discharge (285×10^9 m^3 year^{-1}).[40] The PRE is a typically human-impacted estuary, with an annual input of $\sim 9.0 \times 10^{12}$ kg of industrial and domestic sewages.[41] The abundance, composition, and properties of DOM in the PRE vary significantly from land to sea.[20,42–44] In this study, DOM samples collected from the freshwater, brackish water, and seawater zones of the PRE were irradiated under three spectral regimes of simulated solar radiation to (1) elucidate the spectral (UVB, UVA, and VIS) and spatial variations in the AQYs of DOC photomineralization, CDOM and FDOM photobleaching, and FDOM photoproduction, and (2) assess the relative contributions of solar UVB, UVA, and VIS to these photoprocesses. Results demonstrate that VIS plays unexpectedly important roles in DOC photomineralization and biolabile DOM photoproduction, suggesting profound implications for DOM-related biogeochemical cycles in river-impacted coastal oceans.

2 Methods

2.1 Sample collection

Water sampling was carried out during the dry season (10–14 January) of 2016. *In situ* water temperatures and salinities were recorded using an SBE-25 conductivity-temperature-depth (CTD) profiler (Li *et al.*, 2019).[44] Surface water ($\sim$1 m depth) was collected using a 5 L plexiglass sampler from the head (Sta. M01), the main mixing zone (Sta. M08), and the shelf (Sta. M10) of the PRE (Fig. 1), hereinafter referred to as M01, M08, and M10, respectively. The bulk water was immediately filtered through a 0.2 μm polyethersulfone (PES) filter (Pall Life Sciences) under low vacuum. The filtrate was transferred into a 5 L clear-glass bottle, sealed with Teflon-lined polypropylene caps, stored cold ($\sim$4 °C) in the dark, and transported to the land-based laboratory within one week for photochemical incubations.

Before use, the glass filtration systems and glass bottles had been cleaned sequentially with acid washing, Milli-Q water rinsing, combustion at 450 °C for 4 h. The polypropylene caps had been sequentially acid-washed, Milli-Q water rinsed, and then dried at room temperature. The PES filters had been thoroughly rinsed with Milli-Q water and sample water.

2.2 Irradiation experiments

The filtered samples were warmed up to room temperature in the dark, and re-filtered through 0.2 μm PES filters to further ensure the samples' integrity. Then the fitrate was transferred into 15 quartz-windowed cylindrical cells (volume: 120 mL; height: 13 cm; pre-combusted at 450 °C) and side-sealed free of headspace.[9] Nine cells were wrapped with black electric tape on the sidewalls and bottom to avoid light interference between the cells. The other six cells were completely wrapped with electric tape to serve as dark controls. The sample-filled quartz cells were placed vertically in a temperature-controlled water bath (20 °C) and irradiated for 4 days (d) under a SUNTEST XLS+

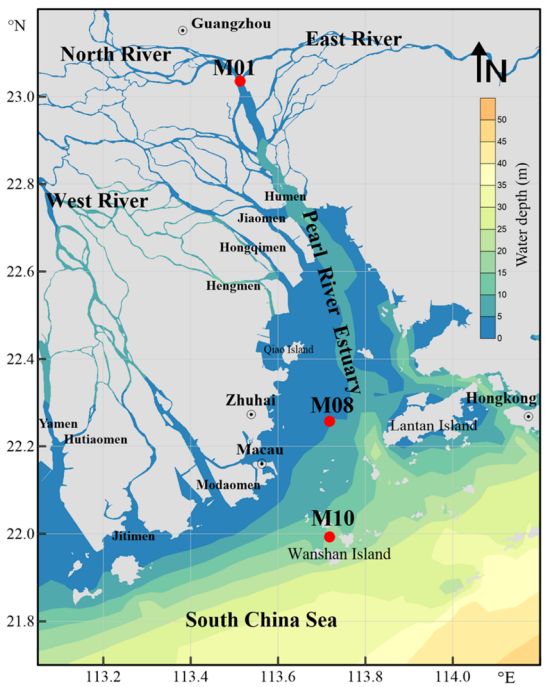

Fig. 1 Map of sampling stations in the Pearl River estuary. Water depths at stations M01, M08, and M10 are 12.0, 6.9, and 20.4 m, respectively.

solar simulator equipped with a 1.5 kW xenon lamp and a UV filter to remove radiation with wavelengths <290 nm. Three spectral light treatments were made by screening the incident light using a quartz plate, a Mylar-D film, and a UF-5 Plexiglas filter to yield full-spectrum (290–700 nm, FS), UVA plus visible (320–700 nm, UVA + VIS), and visible-only (400–700 nm, VIS) irradiation,[16] respectively. The contributions of UVB (290–320 nm) and UVA (320–400 nm) to various DOM photochemical processes were assessed as the differences between FS and UVA + VIS, and between UVA + VIS and VIS,[16] respectively. Light treatments (in triplicate) were accompanied by dark controls (in duplicate). After incubation, all the irradiated and dark-control samples were transferred into 20 mL glass bottles for DOC analysis and into 100 mL glass bottles for determining CDOM absorption and FDOM fluorescence spectra.

Spectral irradiances reaching the top of the quartz cells under each light treatment were measured at 1 nm intervals from 290 to 600 nm using an OL-756 spectroradiometer fitted with an OL IS-270 2-inch integrating sphere calibrated with an OL756-10E irradiance standard (Gooch & Housego, USA).[19] The spectrally integrated irradiances under FS, UVA + VIS and VIS were 376.1, 308.5 and 264.8 W m^{-2} s^{-1}, respectively (Fig. S1). The integrated photon fluxes over the UVB, UVA and VIS were 0.67, 1.71 and 1.64 times those of the monthly-averaged noontime clear-sky solar radiation in January 2016 at 22.5 °N modeled using the SMARTS2 model,[45,46] based on the input conditions shown in Table S1. The 4-d solar-simulated irradiation under FS equaled to 10.8-d UVB, 27.2-d UVA and 26.2-d VIS monthly-averaged clear-sky irradiations in January 2016 at 22.5 °N.

2.3 Sample analysis

The determinations of DOC concentration, CDOM absorption and fluorescence spectra followed the procedure of Yang *et al.* (2020)[9] and Li *et al.* (2019).[44] DOC concentration was measured using a Shimadzu TOC-L_{CPH} analyzer calibrated with standard potassium hydrogen phthalate solutions. Low-carbon water (1–2 μmol L^{-1}) and deep-water reference (41–44 μmol L^{-1}) from D. A. Hansell's laboratory (University of Miami) were analyzed at the intervals of 10 sample analyses to monitor the stability of the analyzer. The measured DOC concentrations were 2.1 ± 0.1 μmol L^{-1} for the low-carbon water reference and 43 ± 1 μmol L^{-1} for the deep-water reference. The coefficient of variation for five replicate sample injections was <2%.

CDOM absorption spectra were determined using a Shimadzu UV-2550 dual-beam spectrophotometer fitted with 10 cm quartz cuvettes and referenced to Milli-Q water. The absorption spectra were scanned from 800 to 200 nm at 1 nm intervals. The average absorbance between 683 and 687 nm was subtracted at each wavelength to remove baseline drifts.[47] The Napierian CDOM absorption coefficient at wavelength λ (nm), $a_{CDOM}(\lambda)$ (m^{-1}), was calculated as follow:

$$a_{CDOM}(\lambda) = 2.303A(\lambda)/L \quad (1)$$

where $A(\lambda)$ is the spectral absorbance at wavelength λ (nm) and L is the light pathlength of the cuvette in meters (0.1 m). Spectral slopes of CDOM absorption between 275 nm and 295 nm ($S_{275–295}$)[48] and between 300 nm and 600 nm ($S_{300–600}$)[49] were derived using nonlinear fitting adapted from the methods of Helms *et al.* (2008)[48] and Stedmon and Markager (2001),[49] respectively. The specific UV absorption coefficient of CDOM at 254 nm ($a^*_{CDOM}(254)$) is calculated by normalizing the Napierian $a_{CDOM}(254)$ by DOC concentration (units: L mg^{-1} m^{-1}).[50] In this study, $a_{CDOM}(330)$, $a^*_{CDOM}(254)$, and $S_{275–295}$ are used as indicators of CDOM abundance,[5,32,51] aromaticity,[50] and molecular weight (MW),[48] respectively. The calculation of spectral slopes over two different wavelength ranges, with $S_{275–295}$ confined to the short-UV band and $S_{300–600}$ covering both the UV and VIS domains, allows for assessing if CDOM photobleaching under the three light treatments (*i.e.*, FS, UVA + VIS, and VIS only) affects the two spectral slopes differently.

Fluorescence excitation–emission matrices (EEMs) were acquired using a Hitachi F-4600 fluorescence spectrophotometer fitted with a 1 cm quartz cell. The excitation wavelength range was 200–450 nm at 5 nm intervals, and the emission spectra were determined from 230 to 600 nm at 2 nm increments. Raman scattering was removed by subtracting the EEMs of Milli-Q water scanned on the same day as those for the samples. The spectral fluorescence intensities were normalized to Raman unites (R.U.) according to Lawaetz and Stedmon (2009),[52] and the potential inner-filtering effects were corrected according to Ohno (2002).[53]

PARAFAC analysis of the EEMs for characterizing FDOM components[54] followed the procedure reported by Li *et al.* (2019).[44] Four FDOM components (C1–C4) were identified by PARAFAC modeling (Fig. 2). C1 and C2 are designated as protein-like FDOM, and C3 and C4 as humic-like FDOM.[3] The strong linear relationships between C1 and C2 ($R^2 = 0.992$, $p < 0.01$, $n = 12$), and between C3 and C4 ($R^2 = 0.973$, $p < 0.05$, $n = 12$), including both the unirradiated and irradiated samples (Fig. S2), indicated similar sources and photochemical behaviors within each FDOM category. To facilitate discussion, the two protein-like components (C1 and C2) were aggregated and denoted as C_P, and the two humic-like components (C3 and C4) as C_H.

Changes of interested parameters (*i.e.*, DOC, $a_{CDOM}(330)$, $S_{275–295}$, $S_{300–600}$, C_P, and C_H) in the dark controls were ≤3% of their initial values and were subtracted from the corresponding light treatments for calculating the photochemical changes.

2.4 Calculation of broadband AQYs

The broadband AQY is defined as the observed photochemical change for a given process over the spectral band of interest divided by the number of photons absorbed by CDOM over that band (Q_{CDOM}, mol photons), which was calculated according to Hu *et al.* (2002):[55]

$$Q_{CDOM} = \text{area} \times t \times \int_{\lambda_1}^{\lambda_2} Q_0(\lambda) \times (a_{CDOM}(\lambda)/a_{total}(\lambda)) \times \left(1 - e^{-a_{total}(\lambda)\times l}\right) \times d\lambda \quad (2)$$

where $Q_0(\lambda)$ is the spectral photon flux reaching the upper water surface inside the quartz cell (mol photons m^{-2} s^{-1} nm^{-1});

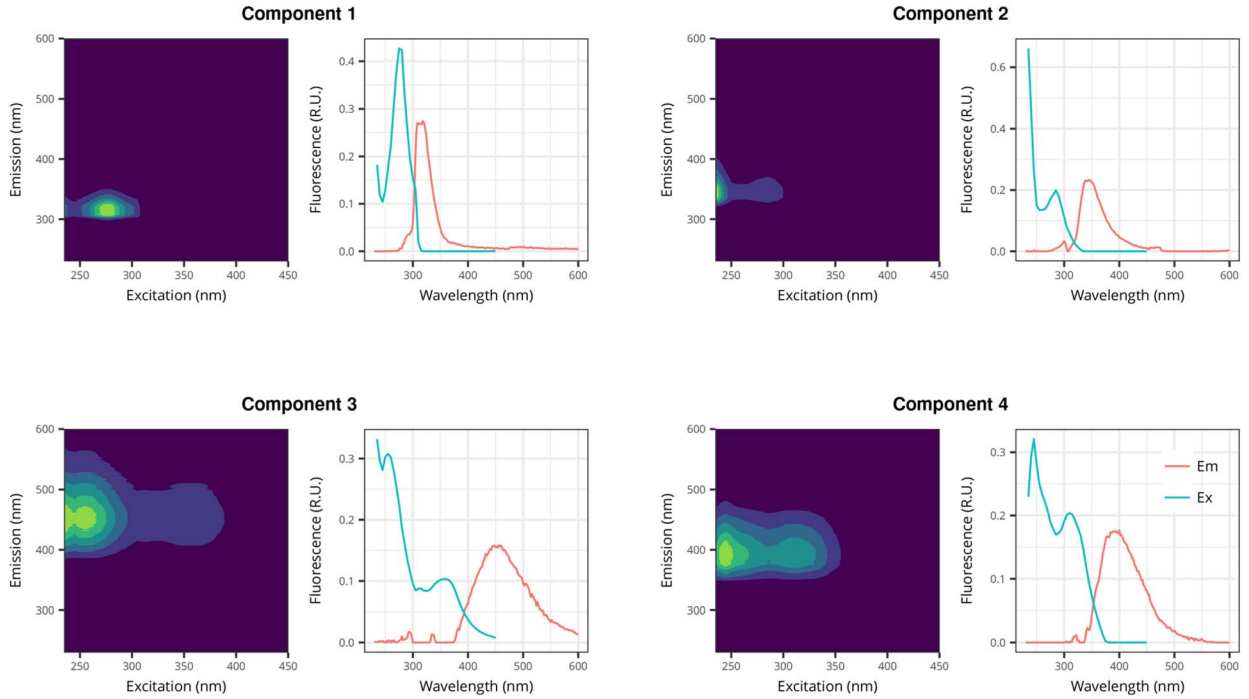

Fig. 2 Excitation–emission contours of four components identified by PARAFAC modeling (left panels) and split-half validations of excitation and emission loadings (right panels). Excitation/emission maximum wavelengths are: C1: 275/320 nm; C2: < 240(280)/340 nm; C3: 260(360)/450 nm; C4: 245(320)/390 nm.

$a_{CDOM}(\lambda)$ the geometric mean of the initial and final absorption coefficients during the 4-d irradiation, assuming that CDOM photobleaching follows first-order kinetics;[56] $a_{total}(\lambda)$ the sum of $a_{CDOM}(\lambda)$ and the absorption coefficient of pure water obtained from Pope and Fry (1997)[57] and Buiteveld *et al.* (1994);[58] λ_1 and λ_2 the lower and upper bound of the integration wavelength range (UVB: 290–320 nm; UVA: 320–400 nm; VIS: 400–600 nm); area the upper surface area of the quartz cell (9.23×10^{-4} m^2); l the light pathlength of the irradiation cell (0.13 m); and t the irradiation duration (4 d). Broadband AQYs were calculated for photochemical removals of DOC (AQY_{DOC}), $a_{CDOM}(330)$ (AQY_{CDOM}), and PARAFAC-modeled humic-like C_H (AQY_{HFDOM}) and protein-like C_P (AQY_{PFDOM}) over the UVB, UVA, and VIS bands, respectively. The units of $a_{CDOM}(\lambda)$ are assigned as m^{-1} m^{-3} and those of C_P, and C_H as R.U. m^{-3} for the AQY calculations according to Vähätalo and Wetzel (2004)[30] and Osburn *et al.* (2009).[32] For brevity, AQY for a specific spectral band will be designated as AQY(band name); for example, AQY_{DOC}(UVB), AQY_{DOC}(UVA), and AQY_{DOC}(VIS) represents the DOC photomineralization AQY over the UVB, UVA, VIS bands, respectively.

2.5 Statistical analyses

MATLAB (version: R2023b) and Ocean Data View (version: 5.5.1) were used for statistical analyses and graph production. Paired two-sample t-tests ($\alpha = 0.05$) assuming unequal variances were performed to determine the significance of difference between two groups. One-tailed probability (p) values and two-tailed p values from the t-tests are shown in Tables S2–S4, and will not be repeated in the text below.

3 Results and discussion

3.1 Properties of original water samples

In situ temperature and salinity both increased seaward from Sta. M01 to Sta. M08 to Sta. M10 (Table 1). The M01 sample was composed of 99.4% freshwater, M08 32.9%, and M10 6.8%, based on a simple mixing model that assumes the salinities of the freshwater and seawater endmembers to be zero and 35, respectively. Hence, the M01 sample can be considered as freshwater, M08 as brackish water, and M10 as being of more marine nature.

DOM variables summarized in Table 1 indicate that (1) DOC, CDOM (proxy: $a_{CDOM}(330)$), protein-like FDOM (proxy: C_P), and humic-like FDOM (proxy: C_H) in the original samples were most abundant in the M01 sample, followed successively by M08 and M10; (2) MW (indicator: $S_{275-295}$) and aromaticity (indicator: $a^*_{CDOM}(254)$) of CDOM showed a similar trend among the three samples, and (3) protein-like FDOM was more abundant than humic-like FDOM (*i.e.*, $C_P/C_H > 1$) in all three samples, with the enrichment in the descending order of M01 > M10 > M08. These results align with other studies showing that: (1) DOM in the PRE is rich in protein-like FDOM, particularly in the head region, due in part to sewage inputs;[59,60] (2) continually dilution of riverine DOM by seawater during its seaward transport;[44,59–62] and (3) faster microbial removal of protein-like FDOM relative to humic-like FDOM in the head region of the estuary;[44,60] (4) a higher proportion of planktonic DOM in the bulk DOM pool over the shelf (M10) relative to the main mixing zone (M08) of the estuary,[43,63,64] as suggested by the higher C_P/C_H over the shelf (Table 1).

Table 1 *In situ* temperature, salinity, dissolved organic carbon (DOC), CDOM absorption coefficient at 330 nm ($a_{CDOM}(330)$), protein-like FDOM (C_P), humic-like FDOM (C_H), specific UV absorption coefficient of CDOM at 254 nm ($a^*_{CDOM}(254)$), spectral slopes of CDOM between 275 nm and 295 nm ($S_{275-295}$) and between 300–600 nm ($S_{300-600}$), and the C_P/C_H ratio of the original (*i.e.*, unirradiated) water samples

	Sta. M01	Sta. M08	Sta. M10
In situ temperature (°C)	17.88	18.89	19.69
Salinity	0.21	23.50	32.61
DOC (μmol L^{-1})	196.3 ± 1.5	91.9 ± 0.3	85.1 ± 1.1
$a_{CDOM}(330)$ (m^{-1})	3.53 ± 0.06	0.88 ± 0.05	0.40 ± 0.02
C_P (R.U.)	3.74 ± 0.02	0.49 ± 0.01	0.15 ± 0.005
C_H (R.U.)	0.86 ± 0.01	0.17 ± 0.01	0.05 ± 0.002
$a^*_{CDOM}(254)$ (L m^{-1} mg^{-1})	5.03 ± 0.10	3.24 ± 0.01	2.03 ± 0.12
$S_{275-295}$ (μm^{-1})	15.8 ± 0.03	19.4 ± 0.03	27.1 ± 0.40
$S_{300-600}$ (μm^{-1})	16.9 ± 0.04	15.6 ± 0.04	10.4 ± 0.06
C_P/C_H	4.36 ± 0.001	2.85 ± 0.002	3.07 ± 0.01

3.2 Photochemical alternations of DOM properties

The three water samples were subjected to varying degrees of self-shading during the irradiation experiments due to different CDOM contents (see $a_{CDOM}(330)$ in Table 1). In addition, self-shading intensified toward short wavelengths, with the visible wavelengths (400–600 nm) exhibiting little self-shading in all three samples (Fig. S3). The variability in self-shading renders it difficult to quantitatively compare different samples and different spectral bands based on photochemical changes unnormalized by absorbed photons.[28,55] This section thus mainly describes intra-sample and intra-spectral band photochemical changes. Quantitative inter-sample and inter-spectral band comparisons can be found in Section 3.3 on AQYs, a quantity normalized by absorbed photons.

FS exposure diminished $a^*_{CDOM}(254)$ in all three samples (Fig. 3A). Under UVA + VIS and VIS-only, $a^*_{CDOM}(254)$ also decreased significantly in the M01 and M08 samples but the change was negligible in M10. $S_{275-295}$ increased in all three samples under FS and UVA + VIS (Fig. 3B). Under VIS-only, $S_{275-295}$ decreased significantly in M10 but essentially remained unchanged in M01 and M08. These results indicate that the aromaticity and MW of CDOM generally declined in the presence of UV, but the effect varied among different samples under VIS-only exposures. Unlike $S_{275-295}$, $S_{300-600}$ decreased in all three samples, under all three light treatments except for a relatively small increase in M01 under FS (Fig. 3C). Notably, the decreases in $S_{300-600}$ under VIS-only were comparable to or larger than those under UVA + VIS and were only moderately smaller than those under FS. This is unexpected given the much lower photon energies in the visible wavelengths than within the UV band. The VIS-induced decreases in $S_{300-600}$ imply that VIS eliminated shortwave absorption faster than it did to longwave absorption on a relative basis, supposedly through optical charge-transfer interactions.[65]

Under FS and UVA + VIS exposures, DOC, $a_{CDOM}(330)$, C_P and C_H significantly decreased in all three samples (Fig. 4A–D), with their relative losses in the descending order of $C_H > C_P \approx a_{330} >$ DOC, similar to the results of previous studies (Bittar *et al.*, 2015; Yang *et al.* 2020).[9,24] VIS exposure led to significant losses of DOC in all three samples (Fig. 4A), and of $a_{CDOM}(330)$ and C_H in the M01 sample but not in M08 and M10 (Fig. 4B and D). Remarkably, VIS exposure resulted in significant increases in C_P (*i.e.*, production of protein-like FDOM) in all three samples (Fig. 4C). Previous studies have demonstrated that microbial labile DOM can be photochemically generated.[9,10,33,66,67] The increase in C_P under VIS observed in the present study suggests that VIS may induce the photoproduction of biolabile, proteinaceous DOM. The mechanism of photoproduction of protein-like FDOM remains unclear. Results from a recent study,[68] however, suggest that photochemical conversion of di-tyrosine, which is likely present in seawater and marine biomass,[68] to tyrosine could be one plausible pathway. Di-tyrosine shows humic-like FDOM characteristics[68] while tyrosine is a typical model compound with fluorescence features of protein-like FDOM in natural waters.[3,69] Note that the loss of C_P under FS and UVA + VIS does not signify the inability of UV to generate protein-like DOM since the decomposition of protein-like FDOM by UV could have overtaken its production by UV and VIS combined in these treatments.[8] In fact, accumulations of

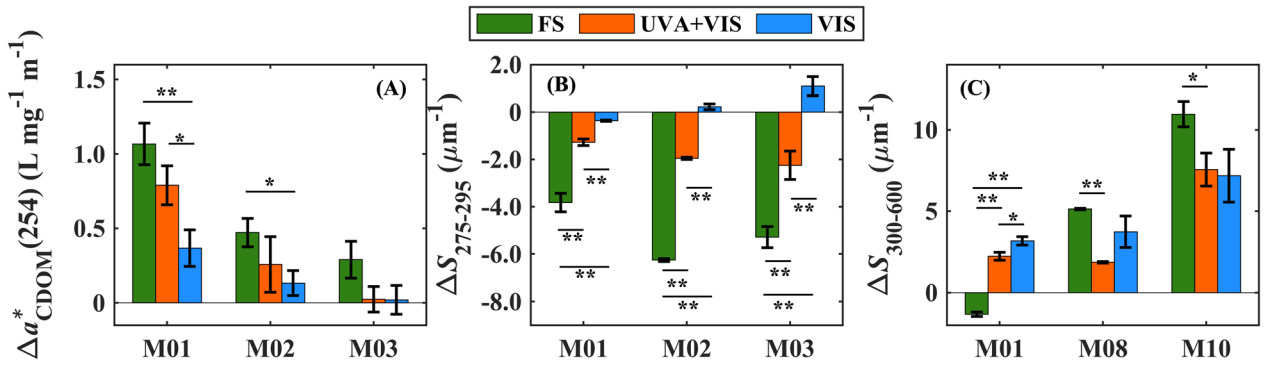

Fig. 3 Absolute changes (dark control minus irradiated) of $a^*_{CDOM}(254)$ (A), $S_{275-295}$ (B), and $S_{300-600}$ (C) after 4-day photochemical incubation under full-spectrum (FS), UVA and visible (UVA + VIS), and visible (VIS) radiation. Positive values denote a decrease, while negative values denote an increase. Error bars represent one standard deviation. * and ** indicate statistically significant differences between different light treatments at $p < 0.05$ and $p < 0.01$, respectively. p values of statistical tests for comparing different samples under UVB, UVA + VIS, and VIS exposure are shown in Table S3.

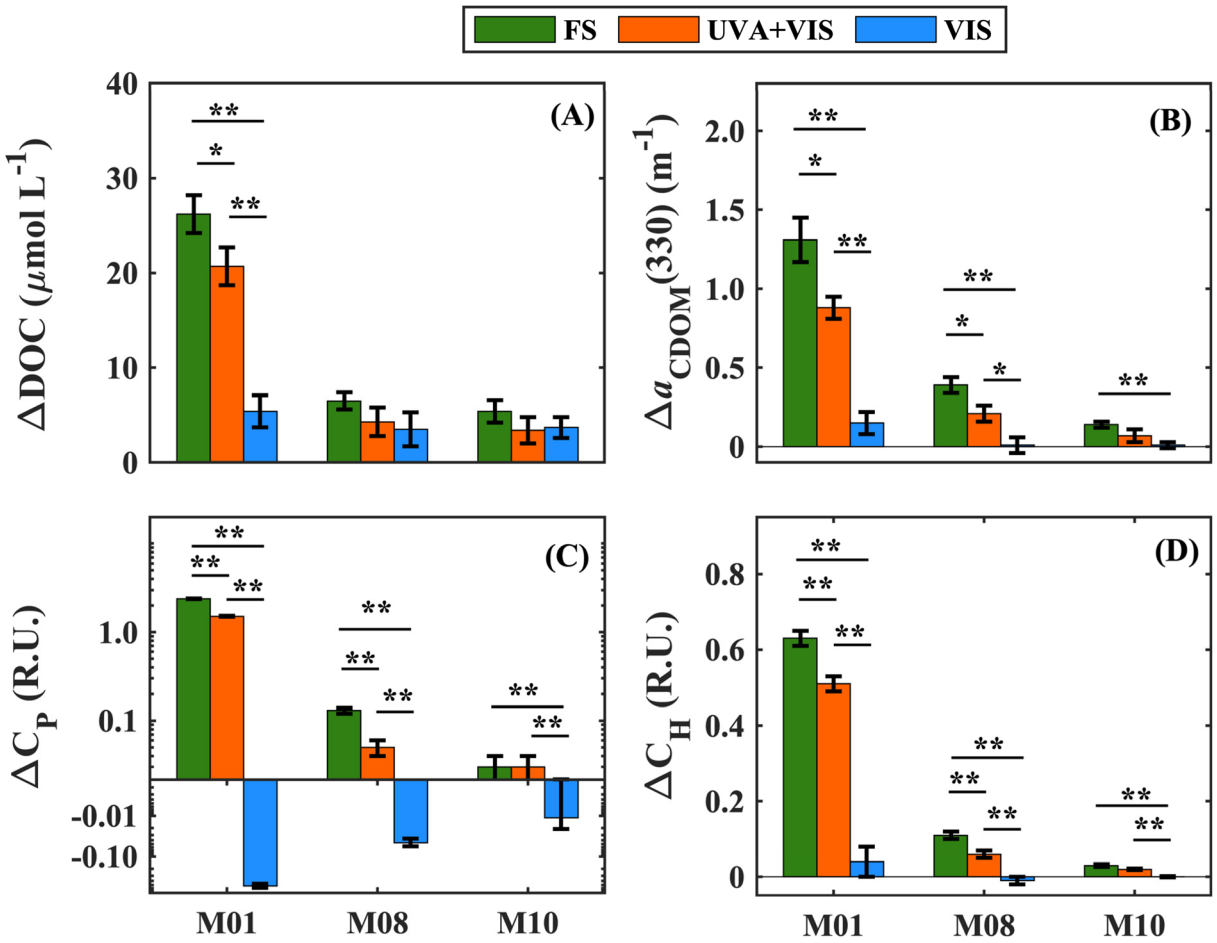

Fig. 4 Absolute changes (dark control minus irradiated) of DOC (A), $a_{CDOM}(330)$ (B), C_P (C) and C_H (D) after 4-day photochemical incubation under full spectrum (FS), UVA and visible (UVA + VIS), and visible (VIS) radiation. Positive values denote a decrease (loss), while negative values denote an increase (production). Note that the *Y*-axis of panel (C) is on logarithmic scale. Error bars represent one standard deviation. * and ** indicate statistically significant differences between different light treatments at $p < 0.05$ and $p < 0.01$, respectively. *p* values of statistical tests for comparing different samples under UVB, UVA + VIS, and VIS exposure are shown in Table S3.

protein-like FDOM under FS exposure have indeed been observed in certain open-ocean water samples,[8,9] suggesting that whether a net production of protein-like FDOM occurs in the presence of UV likely depends on the chemical properties of DOM being irradiated. The mechanisms for VIS-induced photoproduction of protein-like FDOM is unclear. Amino acids and primary amines are known biolabile photoproducts from DOM, including humic substances,[70–72] which are photoreactive under VIS.[36] It remains to be determined whether more complex proteinaceous compounds can be photochemically produced from DOM.

3.3 Broadband AQYs

Among the three spectral bands tested, AQY_{DOC}(UVB) was highest followed sequentially by AQY_{DOC}(UVA) and AQY_{DOC}(VIS) for the M01 sample (Fig. 5A), aligning with previous observations of decreasing AQY_{DOC} with increasing wavelength.[32,73] For M08 and M10, although AQY_{DOC}(UVB) was also the highest, AQY_{DOC}(VIS) was 1.4 (M08) and 3.1 (M10) times AQY_{DOC}(UVA). To our knowledge, this is the first time that VIS is found to be more efficient than UVA at DOC photomineralization, though White *et al.* (2010)[73] reported the AQYs of CO photoproduction to be higher at VIS than at UVA for low-salinity samples in the Delaware estuary. As the shape of AQY_{DOC} is affected by the DOM composition,[27] the seaward decrease of AQY_{DOC}(UVA) but increase of AQY_{DOC}(VIS) (Fig. 5A) could be related to the increasing proportion of planktonic DOM relative to terrestrial and sewage DOM towards the lower estuary.[43,63,64] It is noteworthy that AQY_{DOC}(VIS) co-varied with $\Delta S_{300-600}$ under VIS, both increasing seaward (Fig. 3C and 5A). However, the relationship between the two variables is not significant due to the small number of samples ($r = 0.90$, $p = 0.29$, $n = 3$). Expanded studies are needed to ascertain if $S_{300-600}$ can serve as good metrics for AQY_{DOC}(VIS) and thus facilitate modeling DOC photomineralization rates in natural waters.

DOC photomineralization has long been attributed to photodecarboxylation of carboxylic groups in DOM.[74,75] Both aliphatic and aromatic carboxylic acids containing long-chain conjugate structures possess maximum absorbances in the VIS domain[76,77] and can be decarboxylated under VIS.[76,78]

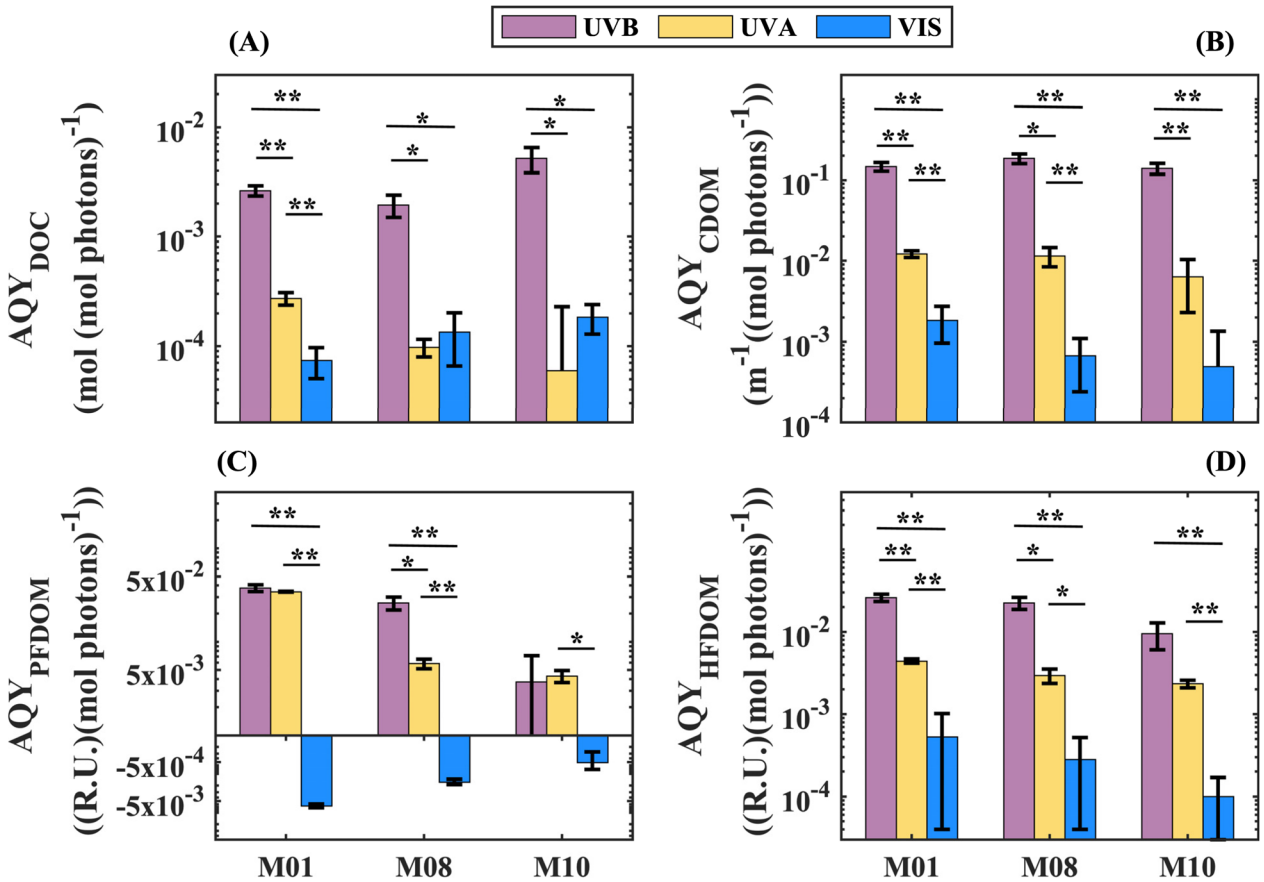

Fig. 5 UVB, UVA, and VIS broadband AQYs of DOC photomineralization (A), CDOM photobleaching represented by $a_{CDOM}(330)$ (B), protein-like FDOM photobleaching or photoproduction represented by C_P (C), and humic-like FDOM photobleaching represented by C_H (D). Negative AQYs (blue bars) in panel (C) indicate photoproduction of protein-like FDOM. Error bars represent one standard deviation. * and ** indicate statistically significant differences between different light treatments at $p < 0.05$ and $p < 0.01$, respectively. p values of statistical tests for comparing different samples under UVB, UVA and VIS exposure are shown in Table S4.

Moreover, the double-bond equivalents (DBE) and carboxylic-rich alicyclic-like molecules (CRAM) in DOM of the PRE increase from the mixing zone to the shelf,[62,79] suggesting that the relative content of unsaturated (*i.e.*, conjugated) carboxylic acids increases seaward. Additionally, iron can accelerate photodecarboxylation under VIS.[80,81] The increasing dissolved iron[82] and CRAM from the mixing zone to the shelf, combined with the maximum VIS absorbances of long-chain conjugate carboxylic acids, may thus lead to higher AQY_{DOC} at VIS than at UVA.

Regarding photobleaching of CDOM and humic-like FDOM, AQY_{CDOM} and AQY_{HFDOM} decreased from UVB to UVA to VIS for all three samples (Fig. 5B and D), consistent with previous studies.[30,39,83] For photobleaching of protein-like FDOM, AQY_{PFDOM}(UVB) was 4.4 times AQY_{PFDOM}(UVA) for M08, while UVB and UVA yielded comparable AQY values for M01 and M10 (Fig. 5C). As the protein-like FDOM was produced under VIS (Section 3.2), its AQYs over VIS refer to the photoproduction efficiency and thus cannot be compared with the photobleaching AQYs over UVB and UVA.

Among the three samples examined, M01 displayed the highest AQY_{DOC}(UVA), AQY_{CDOM}(UVA), and AQY_{CDOM}(VIS), followed in descending order by M08 and M10; the same spatial distribution pattern held for AQY_{HFDOM} and AQY_{PFDOM} across all three spectral regimes (Fig. 5). An opposite inter-samples trend was observed for DOC photomineralization AQYs over VIS (Fig. 5A). On the other occasions, the AQYs were comparable either between all three samples (AQY_{CDOM}(UVB)) or between two of the three samples (AQY_{DOC}(UVB), AQY_{HFDOM}(UVA), and AQY_{PFDOM}(UVA) for M01 and M08).

3.4 Contributions of different spectral regimes to water-column photochemical rates

The depth-integrated photochemical change (*i.e.*, loss or production) rate of a DOM property (DOC, $a_{CDOM}(330)$, C_P, and C_H) in the euphotic zone of the PRE is calculated as the sum of its depth-integrated change rates under UVB, UVA, and VIS:

$$P_T = P_{UVB} + P_{UVA} + P_{VIS} \quad (3)$$

where P_T is the total photochemical change rate of a given DOM property, and P_{UVB}, P_{UVA} and P_{VIS} denote the rates under UVB, UVA and VIS, respectively. P_{UVB}, P_{UVA} and P_{VIS} are calculated as the numbers of photons absorbed by CDOM in the water

column multiplied by the broadband AQYs over the corresponding spectral bands, assuming negligible vertical variations in the AQYs and CDOM absorption coefficients in the euphotic zone. The SMARTS2 model[45,46] (see input parameters in Table S1) was used to derive the monthly mean daily clear-sky spectral solar photon fluxes (290–600 nm) at 22.5 °N in January 2016. The detailed procedure for calculating the photon fluxes absorbed by CDOM is presented in Text S1. The estimated absolute rates for each spectral band and their percent contributions to the total rate are shown in Fig. 6.

For DOC photomineralization, UVB (50.2%) contributed more than did UVA (29.3%) and VIS (20.5%) at Sta. M01, while

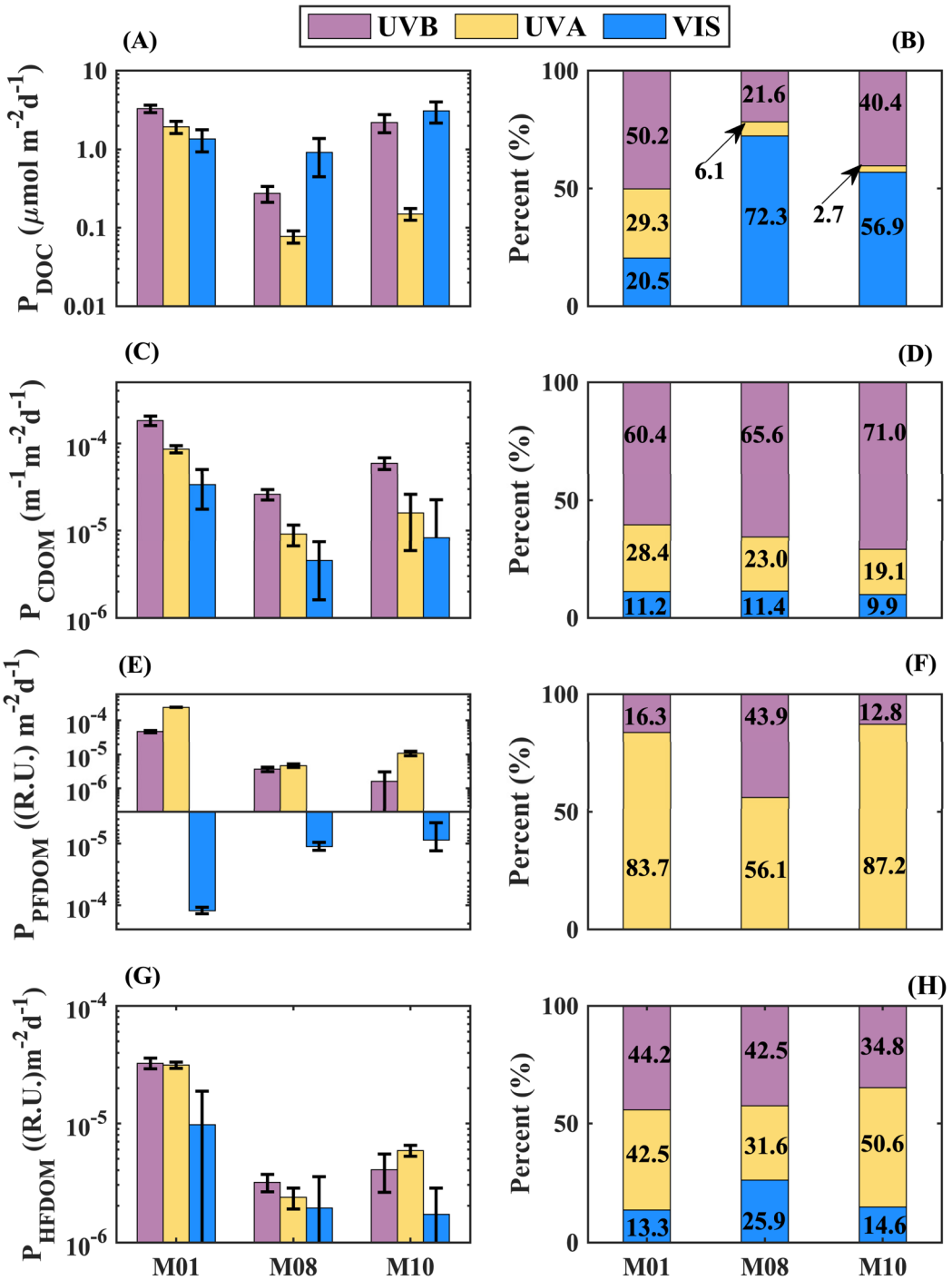

Fig. 6 Modeled absolute changes and percent contributions of UVB, UVA and VIS to the photodegradation of DOC (A and B), $a_{CDOM}(330)$ (C and D), C_P (E and F) and C_H (G and H) in the water column at each station. Negative P_{PFDOM} (blue bars) in panel (E) indicate photoproduction of protein-like FDOM. Note that the contribution of visible light is absent in panel (F) since protein-like FDOM is produced under VIS. The numbers in the bars of the right panels denote the percent contribution values of UVB, UVA and VIS. Error bars in the left panels represent one standard deviation.

VIS was the dominant contributor at both Sta. M08 (72.3%) and Sta. M10 (56.9%), followed by UVB (21.6% and 40.4%) and UVA (6.1% and 2.7%) (Fig. 6B). The 20.5% VIS contribution at Sta. M01 is comparable to those in the Yangtze River estuary (19.6%)[38] and a European lake (23%).[36] The VIS contributions at Sta. M08 and M10 are well above the greatest VIS contribution to DOC photomineralization previously reported for the Saguenay River surface water (44%).[37] Such high VIS contributions contrast with many earlier observations showing that UV played a dominant role in DOC photomineralization.[30,36] The higher VIS contributions to DOC photomineralization at Sta. M08 and M10 can be ascribed to a combination of the relatively higher AQY_{DOC}(VIS) than AQY_{DOC}(UVA) (Fig. 5A) and the larger fractions of photons absorbed by CDOM at VIS than at UV in the water column (Fig. S4C). In contrast to the case at Sta. M08 and M10, the fraction of VIS photons absorbed by CDOM at Sta. M01 is lower than that of UV photons (Fig. S4C), which, in conjunction with the lower AQY_{DOC} at VIS than at UVB and UVA (Fig. 5A), leads to less DOC mineralized by VIS in the water column at this location.

Unlike DOC photomineralization, CDOM and humic-like FDOM photobleaching at all three stations were dominated by UV (290–400 nm) (Fig. 6D and H): UVB contributed 60.5–71.0% and UVA 19.1–28.4% to CDOM photobleaching; UVB contributed 34.8–44.2% and UVA 31.6–50.6% to humic-like FDOM photobleaching, depending on sampling stations. In contrast, VIS only contributed 9.9–11.4% to CDOM photobleaching and 13.2–25.9% to humic-like photobleaching, with the VIS contributions to CDOM photobleaching being within the ranges of those found in the Yangtze River estuary (19.8 ± 0.04%)[38] and temperate lakes in North and South America (6–44%).[39] For protein-like FDOM photobleaching, the UVA contributions (56.1–87.2%) were far more important than the UVB contributions (12.8–43.9%) at all three stations (Fig. 6F). Therefore, the relative contributions of UVA to the photobleaching of both humic- and protein-like FDOM are consistently higher than those to CDOM photobleaching, demonstrating that FDOM photobleaching is more photosensitive to UVA than non-fluorescent CDOM photobleaching. The VIS-induced photoproduction of protein-like FDOM could account for 42.3% and 70.9% of the UV-induced photochemical losses at Sta. M01 and Sta. M10, respectively (Fig. 6E). At Sta. M08, the production surpassed the loss by 35%, suggesting a net photochemical accumulation of proteinaceous DOM in the water column of the main mixing zone.

3.5 Implications for ocean DOM cycling, acidification, and deoxygenation

During riverine discharge through estuaries to coastal zones and to open oceans, the water turbidity continuously decreases due to successive settlement of particles. Consequently, the euphotic zone gradually becomes deeper and more solar radiation can be absorbed by CDOM in the water column, thereby accelerating CDOM photoreactions (Fig. 7). CDOM photobleaching shall be restricted to the upper part of the euphotic zone while DOC photomineralization and proteinaceous (biolabile) DOM photoproduction can be extended to the lower part of the euphotic zone due to faster attenuation of UV than VIS combined with UV-dominated CDOM photobleaching and VIS-dominated DOC photomineralization and biolabile DOM photoproduction (Fig. 7). This vertical photochemistry zonation tends to enhance DOM cycling *via* in part the VIS-induced biolabile DOM photoproduction in the lower part of the euphotic zone, stimulating microbial activities there (Fig. 7).

In river plume-influenced coastal/shelf waters, the upper water column can be entirely stratified or is mixed only to shallow depths due to freshwater input into the surface,[84,85]

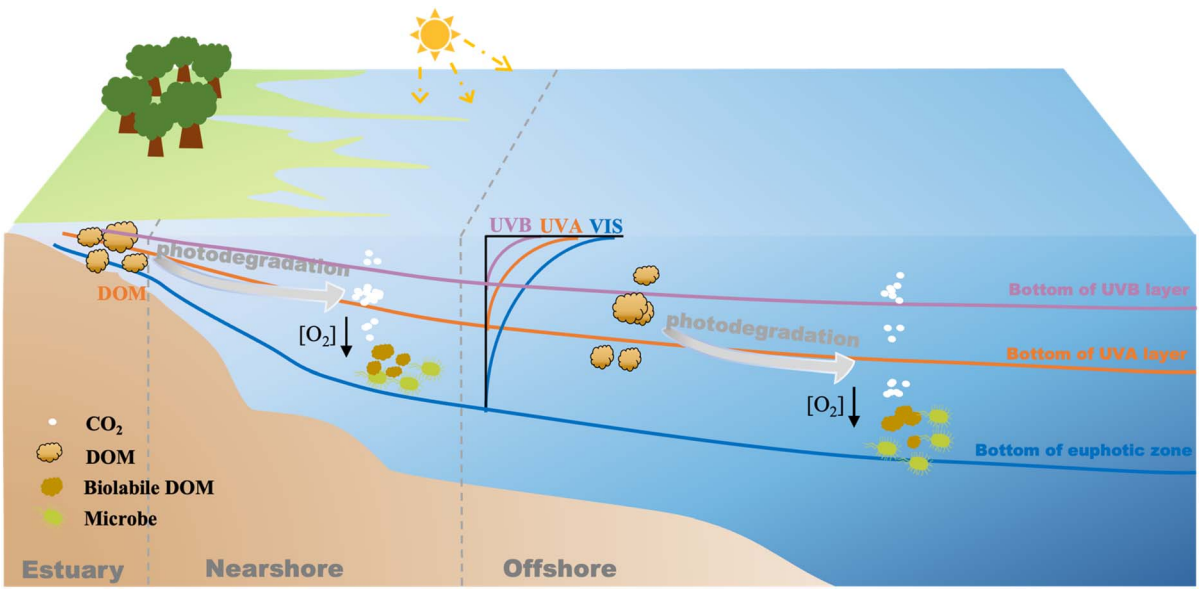

Fig. 7 Conceptual diagram of DOM photodegradation within different optical layers of the euphotic zone along a seaward axis covering estuarine, nearshore, and offshore waters.

causing the euphotic zone to be deeper than the surface mixed layer (SML). Then, DOC photomineralization and biolabile DOM photoproduction may contribute to CO_2 buildup and O_2 consumption in sunlit deeper water, given that both DOC photomineralization and microbial uptake of biolabile DOM consume O_2 and produce CO_2. CDOM photochemistry may, therefore, partly contribute to the increasing acidification and deoxygenation in coastal/shelf waters. Notably, this photochemically induced acidification and deoxygenation (PIAD) shall be a self-intensifying process in the sense that the UV-dominated CDOM photobleaching in surface water allows more VIS to transmit into deeper water. Taking the PRE as an example, summertime O_2 deficiency has been observed at depths as shallow as ~2.5 m below the surface in the lower estuary and surrounding shelf areas (including Sta. M10 in the present study)[86,87] where VIS can penetrate to deeper than 5 m.[88] At Sta. M10 in the shelf area, the 1% VIS penetration depth (*i.e.*, the bottom of the euphotic zone) was estimated to be 5.5 m and the 1% UV penetration depth to be 1.4 m (Text S2). Between depth 1.4 and 5.5 m, the monthy depth-resolved photoproduction rates of protein-like FDOM (P_{PFDOM}) and CO_2 (P_{CO_2}) (approximately equivalent to the DOC photomineralization rate) were calculated using a coupled photochemical-optical model (Text S2 and Fig. S5). At the 2.5 m depth, the estimated monthy P_{PFDOM} and P_{CO_2} in January 2016 were 4.6×10^{-6} R.U. L^{-1} and 1.6 μmol L^{-1}, occupying 3% and 2% of the protein-like FDOM and DOC concentrations at this depth. The monthly photochemical oxygen loss rate (L_{O_2}) was estimated as 1.6–3.2 μmol L^{-1}, assuming the ratio of O_2 consumption to CO_2 production during DOC photomineralization to be 1–2.[75,89,90] As the water temperature in summer (30 °C) is ~10 °C higher than that in winter (20 °C),[44] the DOC photomineralization rate in summer could be 1.3 times that in winter, positing a similar temperature dependence of DOC photomineralization under VIS to that under full spectra.[33] Moreover, the SMART2 model results indicate the solar VIS irradiance in summer is ~1.5 times that in winter. Taking into account the higher water temperature and irradiance yields summertime P_{CO_2} and L_{O_2} of 3.2 μmol L^{-1} and 3.2–6.4 μmol L^{-1}, respectively. The monthly photochemical O_2 consumption rate in summer accounts for 3–6% of the total oxyen consumption (~90–100 μmol L^{-1})[87,91] at 2.5 m over the same time period. Note that the total DOM photochemistry-induced O_2 consumption could be substantially higher since the above estimation does not include the O_2 uptake by microbial degration of the photochemically produced labile DOM under VIS. Additionally, the contribution of photochemical O_2 consumption to total O_2 consumption is expected to further increase seaward due to decreasing suspended particle loads and stronger light penetration.

In a broader context, many areas in open oceans, particularly in the tropics and subtropics, possess a euphotic zone deeper than the SML.[92] PIAD in sunlit subsurface water could be widespread in global oceans if the spectral dependence patterns of the CDOM photoprocesses identified in this study hold for open oceans. Note that PIAD may not be noticeable from vertical profiles of pH and dissolved oxygen if CO_2 consumption and O_2 production by photosynthesis in sunlit subsurface water, often characterized by a subsurface chlorophyll a maximum,[93] may offset or even overtake PIAD. Global warming is expected to enhance PIAD because warmer temperatures tend to strengthen water-column stratification and shoal SMLs.[94] Further studies are needed to verify the existence and significance of PIAD on global ocean scales and assess the impact of climate warming on PIAD.

4 Summary

The photoreactivities of DOM in the freshwater, brackish water, and seawater zones of the PRE were investigated over the UVB, UVA, and VIS domains. In terms of broadband AQY, the efficiencies of UVB-initiated DOC photomineralization and CDOM and humic-like FDOM photobleaching, as expected, are much higher than those initiated by UVA and VIS regardless of sampling locations. The study, however, reveals two previously unrecognized aspects of CDOM photochemistry: VIS dominates DOC photomineralization and leads to proteinaceous DOM photoproduction. As VIS may penetrate the SML, DOC photomineralization and microbial degradation of the photoproduced proteinaceous DOM may cause CO_2 buildup and O_2 depletion below the SML and thus contribute to DOM cycling, acidification, and deoxygenation in river plume-influenced coastal waters. Moreover, the subsurface PIAD is further enhanced as a result of the UV-dominated CDOM photobleaching in surface waters, thereby creating a self-intensifying mechanism. More work is needed to elucidate the broader implications for these biogeochemical cycles in other ocean areas, including open oceans.

Author contributions

G. Song: conceptualization, supervision, methodology, investigation, formal analysis, validation, visualization, writing – original draft, project administration and funding acquisition; F. Niu: investigation, writing – review & editing; Y. Gong: investigation, methodology, formal analysis, validation; P. Massicotte: formal analysis, visualization, methodology, writing – review & editing; H. Zuo: formal analysis; M. Li: formal analysis; H. Xie: conceptualization, supervision, methodology, validation, writing – review & editing.

Conflicts of interest

There are no conflicts to declare.

Data availability

Data are available in the Zenodo.org repository at https://doi.org/10.5281/zenodo.17133706; ref. 95–102 are cited in the supplementary information (SI). Supplementary information is available. See DOI: https://doi.org/10.1039/d5em01004g.

Acknowledgements

We are grateful to the captain and crews of the cruise for their cooperation, R. Li, Z. Shi, M. Chen, Q. Sun, and L. Han for their

help with sampling, and Y. Li and F. Yang for their help in performing the experiments. We thank Professor Y. Li (NNU) for providing their original absorption spectrum of suspended particles and SPM concentrations. Two anonymous reviewers provided constructive comments in improving this manuscript. This work was funded by the National Natural Science Foundation of China (42376039, 42076033).

References

1 C. A. Carlson, and D. A. Hansell, DOM sources, sinks, reactivity, and budgets, in *Biogeochemistry of Marine Dissolved Organic Matter*, ed. D. A. Hansell and C. A. Carlson, Academic Press, Cambridge, MA, 2nd edn, 2015, ch. 3, pp. 65–126.

2 P. G. Coble, J. Lead, A. Baker, D. M. Reynolds, and R. G. M. Spencer, *Aquatic Organic Matter Fluorescence*, Cambridge University Press, New York, NY, 2014.

3 P. G. Coble, Characterization of marine and terrestrial DOM in seawater using excitation-emission matrix spectroscopy, *Mar. Chem.*, 1996, **51**(4), 325–346.

4 K. Mopper, D. J. Kieber, and A. Stubbins, Marine photochemistry of organic matter: processes and impacts, in *Biogeochemistry of Marine Dissolved Organic Matter*, ed. D. A. Hansell and C. A. Carlson, Academic Press, Cambridge, MA, 2nd edn, 2015, ch. 8, pp. 389–450.

5 P. J. Mann, A. Davydova, N. Zimov, R. G. M. Spencer, S. Davydov, E. Bulygina, S. Zimov and R. M. Holmes, Controls on the composition and lability of dissolved organic matter in Siberia's Kolyma River basin, *J. Geophys. Res.*, 2012, **117**, G01028, DOI: 10.1029/2011JG001798.

6 R. M. Cory, K. H. Harrold, B. T. Neilson and G. W. Kling, Controls on dissolved organic matter (DOM) degradation in a headwater stream: the influence of photochemical and hydrological conditions in determining light-limitation or substrate-limitation of photo-degradation, *Biogeosciences*, 2015, **12**, 6669–6685.

7 F. Cao, P. M. Medeiros and W. L. Miller, Optical characterization of dissolved organic matter in the Amazon River plume and the adjacent ocean: examining the relative role of mixing, photochemistry, and microbial alterations, *Mar. Chem.*, 2016, **186**, 178–188.

8 F. Cao, Y. Zhu, D. J. Kieber and W. L. Miller, Distribution and photo-reactivity of chromophoric and fluorescent dissolved organic matter in the northeastern North Pacific Ocean, *Deep Sea Res., Part I*, 2020, **155**, 103168, DOI: 10.1016/j.dsr.2019.103168.

9 F. Yang, G. Song, P. Massicotte, H. Wei and H. Xie, Depth-resolved photochemical lability of dissolved organic matter in the western tropical Pacific Ocean, *J. Geophys. Res.:Biogeosci.*, 2020, **125**, e2019JG005425, DOI: 10.1029/2019JG005425.

10 D. J. Kieber, J. McDaniel and K. Mopper, Photochemical source of biological substrates in sea water: implications for carbon cycling, *Nature*, 1989, **341**, 637–639.

11 W. L. Miller and R. G. Zepp, Photochemical production of dissolved inorganic carbon from terrestrial organic matter: Significance to the oceanic organic carbon cycle, *Geophys. Res. Lett.*, 1995, **22**(4), 417–420.

12 M. A. Moran and R. G. Zepp, Role of photoreactions in the formation of biologically labile compounds from dissolved organic matter, *Limnol. Oceanogr.*, 1997, **42**(6), 1307–1316.

13 K. Kaiser, R. Benner and R. M. W. Amon, The fate of terrigenous dissolved organic carbon on the Eurasian shelves and export to the North Atlantic, *J. Geophys. Res.:Oceans*, 2017, **122**, 4–22.

14 Y. Shen and R. Benner, Mixing it up the ocean carbon cycle and the removal of refractory dissolved organic carbon, *Sci. Rep.*, 2018, **8**, 2542, DOI: 10.1038/s41598-018-20857-5.

15 S. S. Andrews, S. Caron and O. C. Zafiriou, Photochemical oxygen consumption in marine waters: A major sink for colored dissolved organic matter?, *Limnol. Oceanogr.*, 2000, **45**(2), 267–277.

16 T. Lou and H. Xie, Photochemical alteration of the molecular weight of dissolved organic matter, *Chemosphere*, 2006, **65**, 2333–2342.

17 V. Kitidis, G. H. Tilstone, P. Serret, T. J. Smyth, R. Torres and C. Robinson, Oxygen photolysis in the Mauritanian upwelling: Implications for net community production, *Limnol. Oceanogr.*, 2014, **59**(2), 299–310.

18 B. Koehler, E. Broman and L. J. Tranvik, Apparent quantum yield of photochemical dissolved organic carbon mineralization in lakes, *Limnol. Oceanogr.*, 2016, **61**, 2207–2221.

19 G. Song, Y. Li, S. Hu, G. Li, R. Zhao, X. Sun and H. Xie, Photobleaching of chromophoric dissolved organic matter (CDOM) in the Yangtze River estuary: kinetics and effects of temperature, pH, and salinity, *Environ. Sci.: Processes Impacts*, 2017, **19**, 861–873.

20 M. Li, G. Song and H. Xie, Bio- and photo-lability of dissolved organic matter in the Pearl River (Zhujiang) estuary, *Mar. Pollut. Bull.*, 2022, **174**, 113300, DOI: 10.1016/j.marpulbul.2021.113300.

21 C. Grasset, K. Einarsdottir, N. Catalán, L. J. Tranvik, M. Groeneveld, J. A. Hawkes and K. Attermeyer, Decreasing photoreactivity and concurrent change in dissolved organic matter composition with increasing inland water residence time, *Global Biogeochem. Cycles*, 2024, **38**, e2023GB007989, DOI: 10.1029/2023GB007989.

22 C. L. Logvinova, K. E. Frey, P. J. Mann, A. Stubbins and R. G. M. Spencer, Assessing the potential impacts of declining Arctic sea ice cover on the photochemical degradation of dissolved organic matter in the Chukchi and Beaufort Seas, *J. Geophys. Res.:Biogeosci.*, 2015, **120**, 2326–2344.

23 T. B. Bittar, A. Stubbins, A. A. H. Vieira and K. Mopper, Characterization and photodegradation of dissolved organic matter (DOM) from a tropical lake and its dominant primary producer, the cyanobacteria *Microcystis aeruginosa*, *Mar. Chem.*, 2015, **177**, 205–217.

24 T. B. Bittar, A. A. H. Vieira, A. Stubbins and K. Mopper, Competition between photochemical and biological degradation of dissolved organic matter from the

cyanobacteria Microcystis aeruginosa, *Limnol. Oceanogr.*, 2015, **60**, 1172–1194.

25 H. Gao and R. G. Zepp, Factors influencing photoreactions of dissolved organic matter in a coastal river of the southeastern United States, *Environ. Sci. Technol.*, 1998, **32**, 2940–2946.

26 M. Gonsior, B. M. Peake, W. T. Cooper, D. Podgorski, J. D'Andrilli and W. J. Cooper, Photochemically induced changes in DOM identified by ultrahigh resolution Fourier transform ion cyclotron resonance mass spectrometry, *Environ. Sci. Technol.*, 2009, **43**(3), 698–703.

27 J. C. Bowen, C. P. Ward, G. W. Kling and R. M. Cory, Arctic amplification of global warming strengthened by sunlight oxidation of permafrost carbon to CO_2, *Geophys. Res. Lett.*, 2020, **47**, e2020GL087085, DOI: 10.1029/2020GL087085.

28 M. C. Rieb, C. A. Polik, G. W. Kling and R. M. Cory, Controls on the apparent quantum yield for photomineralization of dissolved organic matter in Arctic freshwaters, *Environ. Sci.: Processes Impacts*, 2025, **27**, 2755, DOI: 10.1039/d5em00293a.

29 S. C. Johannessen and M. L. Miller, Quantum yield for the photochemical production of dissolved inorganic carbon in seawater, *Mar. Chem.*, 2001, **76**, 271–283.

30 A. V. Vähätalo and R. G. Wetzel, Photochemical and microbial decomposition of chromophoric dissolved organic matter during long (months–years) exposures, *Mar. Chem.*, 2004, **89**, 313–326.

31 A. V. Vähätalo and R. G. Zepp, Photochemical mineralization of dissolved organic nitrogen to ammonium in the Baltic Sea, *Environ. Sci. Technol.*, 2005, **39**, 6985–6992.

32 C. L. Osburn, L. Retamal and W. F. Vincent, Photoreactivity of chromophoric dissolved organic matter transported by the Mackenzie River to the Beaufort Sea, *Mar. Chem.*, 2009, **115**, 10–20.

33 H. Aarnos, P. Ylöstalo and A. V. Vähätalo, Seasonal phototransformation of dissolved organic matter to ammonium, dissolved inorganic carbon, and labile substrates supporting bacterial biomass across the Baltic Sea, *J. Geophys. Res.*, 2012, **117**, G01004, DOI: 10.1029/2010JG001633.

34 B. Koehler, T. Landelius, G. A. Weyhenmeyer, N. Machida and L. J. Tranvik, Sunlight-induced carbon dioxide emissions from inland waters, *Global Biogeochem. Cycles*, 2014, **28**, 696–711.

35 T. Cai, X. Zhang, S. Zhang, Y. Ming and Q. Zhang, Photochemical behaviors of dissolved organic matter in aquatic environment: generation, characterization, influencing factors and practical application, *Environ. Res.*, 2023, **231**, 116174, DOI: 10.1016/j.envres.2023.116174.

36 A. V. Vähätalo, M. Salkinoja-Salonen, P. Taalas and K. Salonen, Spectrum of the quantum yield for photochemical mineralization of dissolved organic carbon in a humic lake, *Limnol. Oceanogr.*, 2000, **45**(3), 664–676.

37 Y. Zhang and H. Xie, Photomineralization and photomethanification of dissolved organic matter in Saguenay River surface water, *Biogeosciences*, 2015, **12**, 6823–6836.

38 X. Sun, G. Song and H. Xie, The apparent quantum yields of dissolved organic matter photobleaching and photomineralization in the Changjiang River estuary, *Haiyang Xuebao*, 2016, **38**(4), 120–129.

39 C. L. Osburn, H. E. Zagarese, D. P. Morris and B. R. Hargreaves, Calculation of spectral weighting functions for the solar photobleaching of chromophoric dissolved organic matter in temperate lakes, *Limnol. Oceanogr.*, 2001, **46**(6), 1455–1467.

40 X. Wei and C. Wu, Long-term process-based morphodynamic modeling of the Pearl River Delta, *Ocean Dyn.*, 2014, **64**, 1753–1765.

41 X. Peng, S. Xiong, W. Ou, Z. Wang, J. Tan, J. Jin, C. Tang, J. Liu and Y. Fan, Persistence, temporal and spatial profiles of ultraviolet absorbents and phenolic personal care products in riverine and estuarine sediment of the Pearl River catchment, China, *J. Hazard. Mater.*, 2017, **323**, 139–146.

42 J. Callahan, M. Dai, R. Chen, X. Li, Z. Lu and W. Huang, Distribution of dissolved organic matter in the pearl river estuary, China, *Mar. Chem.*, 2004, **89**, 211–224.

43 F. Ye, W. Guo, G. Wei and G. Jia, The sources and transformations of dissolved organic matter in the Pearl River Estuary, China, as revealed by stable isotopes, *J. Geophys. Res.:Oceans*, 2018, **123**, 6893–6908.

44 Y. Li, G. Song, P. Massicotte, F. Yang, R. Li and H. Xie, Distribution, seasonality, optical characteristics, and fluxes of dissolved organic matter (DOM) in the Pearl River (Zhujiang) estuary, China, *Biogeosciences*, 2019, **16**, 2751–2770.

45 C. Gueymard, *SMARTS (Version 2.9.5), SMARTS, A Simple Model of the Atmospheric Radiative Transfer of Sunshine: Algorithms and Performance Assessment*. *Professional Paper FSEC-PF-270-95*, Florida Solar Energy Center, FL, 1995.

46 C. Gueymard, Parameterized Transmittance Model for Direct Beam and Circumsolar Spectral Irradiance, *Sol. Energy*, 2001, **71**(5), 325–346.

47 M. Babin, D. Stramski, G. M. Ferrari, H. Claustre, A. Bricaud, G. Obolensky and N. Hoepffner, Variations in the light absorption coefficients of phytoplankton, nonalgal particles, and dissolved organic matter in coastal waters around Europe, *J. Geophys. Res.*, 2003, **108**(C7), 3211, DOI: 10.1029/2001JC000882.

48 J. R. Helms, A. Stubbins, J. D. Ritchie, E. C. Minor, D. J. Kieber and K. Mopper, Absorption spectral slopes and slope ratios as indicators of molecular weight, source, and photobleaching of chromophoric dissolved organic matter, *Limnol. Oceanogr.*, 2008, **53**(3), 955–969.

49 C. A. Stdemon and S. Markager, The optics of chromophoric dissolved organic matter (CDOM) in the Greenland Sea: An algorithm for differentiation between marine and terrestrial derived organic matter, *Limnol. Oceanogr.*, 2001, **46**(8), 2087–2093.

50 J. L. Weishaar, G. R. Aiken, B. A. Bergamaschi, M. S. Fram, R. Fujii and K. Mopper, Evaluation of specific ultraviolet

absorbance as an indicator of the chemical composition and reactivity of dissolved organic carbon, *Environ. Sci. Technol.*, 2003, **37**, 4702–4708.
51 G. Song, F. Yang, P. Massicotte, H. Wei and H. Xie, CDOM spectral slope ($S_{275\text{-}295}$) as tracers of water masses, CDOM heterogeneity, and Δ^{14}C-DOC in an oligotrophic marginal sea, *Limnol. Oceanogr. Lett.*, 2023, **8**, 789–798.
52 A. J. Lawaetz and C. A. Stedmon, Fluorescence intensity calibration using the Raman scatter peak of water, *Appl. Spectrosc.*, 2009, **63**(8), 936–940.
53 T. Ohno, Fluorescence inner-filtering correction for determining the humification index of dissolved organic matter, *Environ. Sci. Technol.*, 2002, **36**(4), 742–746.
54 C. A. Stedmon and R. Bro, Characterizing dissolved organic matter fluorescence with parallel factor analysis: a tutorial, *Limnol. Oceanogr.:Methods*, 2008, **6**, 572–579.
55 C. Hu, F. E. Muller-Karger and R. G. Zepp, Absorbance, absorption coefficient, and apparent quantum yield: A comment on common ambiguity in the use of these optical concepts, *Limnol. Oceanogr.*, 2002, **47**(4), 1261–1267.
56 R. Del Vecchio and N. V. Blough, Photobleaching of chromophoric dissolved organic matter in natural waters: kinetics and modeling, *Mar. Chem.*, 2002, **78**, 231–253.
57 R. M. Pope and E. S. Fry, Absorption spectrum (380–700 nm) of pure water. II. Integrating cavity measurements, *Appl. Opt.*, 1997, **36**(33), 8710–8723.
58 H. Buiteveld, J. M. H. Hakvoort and M. Donze, The optical properties of pure water, *SPIE Proceedings on Ocean Optics XII*, 1994, 2258, pp. 174–183.
59 H. Hong, J. Wu, S. Shang and C. Hu, Absorption and fluorescence of chromophoric dissolved organic matter in the Pearl River estuary, south China, *Mar. Chem.*, 2005, **97**, 78–89.
60 B. He, M. Dai, W. Zhai, L. Wang, K. Wang, J. Chen, J. Lin, A. Han and Y. Xu, Distribution, degradation and dynamics of dissolved organic carbon and its major compound classes in the pearl river estuary, China, *Mar. Chem.*, 2010, **119**, 52–64.
61 M. Xie, M. Chen and W.-X. Wang, Spatial and temporal variations of bulk and colloidal dissolved organic matter in a large anthropogenically perturbed estuary, *Environ. Pollut.*, 2018, **243**, 1528–1538.
62 Y. Liu, Q. Ye, W.-L. Huang, L. Feng, Y.-H. Wang, Z. Xie, S.-S. Yong, S. Zhang, B. Jiang and J.-J. Wang, Spectroscopic and molecular-level characteristics of dissolved organic matter in the Pearl River estuary, south China, *Sci. Total Environ.*, 2020, **710**, 136307, DOI: 10.1016/j.scitotenv.2019.136307.
63 K. Wu, M. Dai, X. Li, F. Meng, J. Chen and J. Lin, Dynamics and production of dissolved organic carbon in a large continental shelf system under the influence of both river plume and coastal upwelling, *Limnol. Oceanogr.*, 2017, **62**, 973–988.
64 X. Li, Z. Liu, W. Chen, L. Wang, B. He, S. Gu, P. Jiang, B. Huang and M. Dai, Production and transformation of dissolved and particulate organic matter as indicated by amino acids in the Pearl River estuary, China, *J. Geophys. Res.:Biogeosci.*, 2018, **123**, 3523–3537.
65 R. Del Vecchio and N. V. Blough, On the origin of the optical properties of humic substances, *Environ. Sci. Technol.*, 2004, **38**(14), 3885–3891.
66 W. L. Miller, M. A. Moran, W. M. Sheldon, R. G. Zepp and S. Opsahl, Determination of apparent quantum yield spectra for the formation of biologically labile photoproducts, *Limnol. Oceanogr.*, 2002, **47**(2), 343–352.
67 J. Hu, L. Kang, Z. Li, X. Feng, C. Liang, Z. Wu, W. Zhou, X. Liu, Y. Yang and L. Chen, Photo-produced aromatic compounds stimulate microbial degradation of dissolved organic carbon in thermokarst lakes, *Nat. Commun.*, 2023, **14**, 3681, DOI: 10.1038/s41467-023-39432-2.
68 R. W. Paerl, I. M. Claudio, M. R. Shields, T. S. Bianchi and C. L. Osburn, Dityrosine formation via reactive oxygen consumption yields increasingly recalcitrant humic-like fluorescent organic matter in the ocean, *Limnol. Oceanogr. Lett.*, 2020, **5**, 337–345.
69 K. R. Murphy, C. A. Stedmon, T. D. Waite and G. M. Ruiz, Distinguishing between terrestrial and autochthonous organic matter sources in marine environments using fluorescence spectroscopy, *Mar. Chem.*, 2008, **108**, 40–58.
70 N. O. G. Jørgensen, L. Tranvik, H. Edling, W. Granéli and M. Lindell, Effects of sunlight on occurrence and bacterial turnover of specific carbon and nitrogen compounds in lake water, *FEMS Microbiol. Ecol.*, 1998, **25**(3), 217–227.
71 K. L. Bushaw-Newton and M. A. Moran, Photochemical formation of biologically available nitrogen from dissolved humic substances in coastal marine systems, *Aquat. Microb. Ecol.*, 1999, **18**, 285–292.
72 D. J. Koopmans and D. A. Bronk, Photochemical production of dissolved inorganic nitrogen and primary amines from dissolved organic nitrogen in waters of two estuaries and adjacent surficial groundwaters, *Aquat. Microb. Ecol.*, 2002, **26**, 295–304.
73 E. M. White, D. J. Kieber, J. Sherrard, W. L. Miller and K. Mopper, Carbon dioxide and carbon monoxide photoproduction quantum yields in the Delaware estuary, *Mar. Chem.*, 2010, **118**, 11–21.
74 C. J. Miles and P. L. Brezonik, Oxygen consumption in humic-colored waters by a photochemical ferrous-ferric catalytic cycle, *Environ. Sci. Technol.*, 1981, **15**(9), 1089–1095.
75 H. Xie, O. C. Zafiriou, W.-J. Cai, R. G. Zepp and Y. Wang, Photooxidation and its effects on the carboxyl content of dissolved organic matter in two coastal rivers in the southeastern United States, *Environ. Sci. Technol.*, 2004, **38**, 4113–4119.
76 B. Yan, W. Wang and Y. Song, hotophysical properties of praseodymium complexes with aromatic carboxylic acids: Double light conversion both in ultraviolet and visible region, *Spectrochim. Acta, Part A*, 2007, **66**, 11151121, DOI: 10.1016/j.saa.2006.05.024.
77 N. P. Ramirez, B. König and J. C. Gonzalez-Gomez, Decarboxylative cyanation of aliphatic carboxylic acids via

visible-light flavin photocatalysis, *Org. Lett.*, 2019, **21**, 1368–1373.
78 X. Zhang, W. Weng, H. Liang, H. Yang and B. Zhang, Visible-light-initiated, photocatalyst-free decarboxylative coupling of carboxylic acids with N-heterocycles, *Org. Lett.*, 2018, **20**, 4686–4690.
79 C. He, Q. Pan, P. Li, W. Xie, Z. He, C. Zhang and Q. Shi, Molecular composition and spatial distribution of dissolved organic matter (DOM) in the Pearl River estuary, China, *Environ. Chem.*, 2019, **17**, 240–251.
80 B. C. Gilbert, J. R. L. Smith, A. F. Parsons and P. K. Setchell, Photo-decarboxylation of iron(III) porphyrin-amino acid complexes in aqueous solution, *J. Chem. Soc., Perkin Trans. 2*, 1997, **6**, 1065–1073.
81 J. Qian, Y. Zhang, W. Zhao and P. Hu, Decarboxylative halogenation of aliphatic carboxylic acids catalyzed by iron salts under visible light, *Chem. Commun.*, 2024, **60**, 2764–2767.
82 R. Zhang, X. Zhu, C. Yang, L. Ye, G. Zhang, J. Ren, Y. Wu, S. Liu, J. Zhang and M. Zhou, Distribution of dissolved iron in the Pearl River (Zhujiang) estuary and the northern continental slope of the South China Sea, *Deep Sea Res., Part II*, 2019, **167**, 14–24.
83 R. F. Whitehead, S. de Mora, S. Demer, M. Gosselin, P. Monfort and B. Mostajir, Interactions of ultraviolet-B radiation, mixing, and biological activity on photobleaching of natural chromophoric dissolved organic matter: A mesocosm study, *Limnol. Oceanogr.*, 2000, **45**(2), 278–291.
84 Z. Zhu, W.-M. Ng, S. Liu, J. Zhang, J.-C. Chen and Y. Wu, Estuarine phytoplankton dynamics and shift of limiting factors: A study in the Changjiang (Yangtze River) estuary and adjacent area, *Estuarine, Coastal Shelf Sci.*, 2009, **84**, 393–401.
85 O. Pasqueron de Formmervault, P. Perez-Brunius, P. Damien, V. F. Camacho-Ibar and J. Sheinbaum, Temporal variability of chlorophyll distribution in the Gulf of Mexico: bio-optical data from profiling floats, *Biogeosciences*, 2017, **14**, 5647–5662.
86 J. Su, M. Dai, B. He, L. Wang, J. Gan, X. Guo, H. Zhao and F. Yu, Tracing the origin of the oxygen-consuming organic matter in the hypoxic zone in a large eutrophic estuary: the lower reach of the Pearl River estuary, China, *Biogeosciences*, 2017, **14**, 4085–4099.
87 W. Qian, J. Gan, J. Liu, B. He, Z. Lu, X. Guo, D. Wang, L. Guo, T. Huang and M. Dai, Current status of emerging hypoxia in a eutrophic estuary: the lower reach of the Pearl River estuary, China, *Estuarine, Coastal Shelf Sci.*, 2018, **205**, 58–67.
88 H. Ye, C. Chen, Z. Sun, S. Tang, X. Song, C. Yang, L. Tan and F. Liu, Estimation of the primary productivity in Pearl River estuary using MODIS data, *Estuaries Coasts*, 2015, **38**, 506–518.
89 R. M. Amon and R. Benner, Photochemical and microbial consumption of dissolved organic carbon and dissolved oxygen in the Amazon River system, *Geochim. Cosmochim. Acta*, 1996, **60**(10), 1783–1792.
90 C. P. Ward and R. M. Cory, Assessing the prevalence, products, and pathways of dissolved organic matter partial photo-oxidation in Arctic surface waters, *Environ. Sci.: Processes Impacts*, 2020, **22**, 1214–1223.
91 B. He, M. Dai, W. Zhai, X. Guo and L. Wang, Hypoxia in the upper reaches of the Pearl River estuary and its maintenance mechanisms: A synthesis based on multiple year observations during 2000–2008, *Mar. Chem.*, 2014, **167**, 13–24.
92 D. J. Clements, S. Yang, T. Weber, A. M. P. McDonnell, R. Kiko, L. Stemmann and D. Bianchi, New estimate of organic carbon export from optical measurements reveals the role of particle size distribution and export horizon, *Global Biogeochem. Cycles*, 2023, **37**, e2022GB007633, DOI: 10.1029/2022GB007633.
93 S. Yasunaka, T. Ono, K. Sasaoka and K. Sato, Global distribution and variability of subsurface chlorophyll *a* concentrations, *Ocean Sci.*, 2022, **18**, 255–268.
94 M. Roch, P. Brandt and S. Schmidtko, Recent large-scale mixed layer and vertical stratification maxima changes, *Front. Mar. Sci.*, 2023, **10**, 1277316, DOI: 10.3389/fmars.2023.1277316.
95 A. Stubbins, G. Uher, C. S. Law, K. Mopper, C. Robinson and R. C. Upstill-Goddard, Open-ocean carbon monoxide photoproduction, *Deep Sea Res., Part II*, 2006, **53**, 1695–1705.
96 R. Li, J. Xu, X. Li, Z. Shi and P. J. Harrison, Spatiotemporal variability in phosphorus species in the Pearl River estuary: Influence of the river discharge, *Sci. Rep.*, 2017, **7**, 13649, DOI: 10.1038/s41598-017-13924-w.
97 S. Wang, Y. Wang, Q. Fu, B. Yin and Y. Li, Spectral absorption properties of the water constituents in the estuary of Zhujiang River, *Environ. Sci.*, 2014, **35**(12), 4511–4521.
98 W. L. Miller and M. A. Moran, Interaction of photochemical and microbial processes in the degradation of refractory dissolved organic matter from a coastal marine environment, *Limnol. Oceanogr.*, 1997, **42**(6), 1317–1324.
99 A. Morel, Optical properties of pure water and pure seawater, in *Optical Aspects of Oceanography*, ed. N. G. Jerlov, and E. S. Nielsen, Academic Press, New York, 1974, ch. 1, pp. 1–24.
100 A. Vodacek, S. A. Green and N. V. Blough, An experimental model of the solar-stimulated fluorescence of chromophoric dissolved organic matter, *Limnol. Oceanogr.*, 1994, **39**(1), 1–11.
101 S. Buckley, F. Leresche, K. Norris and F. L. Rosario-Ortiz, Role of direct and sensitized photolysis in the photomineralization of dissolved organic matter and model chromophores to carbon dioxide, *Environ. Sci. Technol.*, 2024, **58**(31), 13808–13819.
102 C. Gueymard, The sun's total and spectral irradiance for solar energy applications and solar radiation models, *Sol. Energy*, 2004, **76**, 423–453.